Anomalous scattering for small-molecule crystallography

Madeleine Helliwell

*Department of Chemistry, University of Manchester, Oxford Road, Manchester M13 9PL, UK.
E-mail: mad@pec6.sc.ch.man.ac.uk*

Anomalous dispersion techniques in small-molecule crystallography have been used in recent years with the advent of intense tunable X-radiation from synchrotron X-ray sources. By tuning the wavelength of the radiation close to the absorption edges of specific elements, it is possible to identify and distinguish between atoms which are close together in atomic number, even when two or more such atoms occupy a single site. Anomalous dispersion techniques can also be used to distinguish between valence states of different sites of an element by the valence contrast method or to determine the coordination geometry of an atom. In some cases, when the coordination of an atom is asymmetric, the absorption-edge position may depend on the orientation of the crystal. Finally, anomalous dispersion techniques can be used for *ab initio* structure solution from powder diffraction data. The properties of microporous materials often depend on the incorporation of metal atoms into the framework. Two or more metal atoms close together in atomic number may be incorporated, sometimes occupying a single site. In one study the site of an Ni atom in the aluminophosphate NiAPO was determined by anomalous dispersion techniques and data from the NSLS. Also, the location of the isomorphously substituted cobalt over two crystallographically different zinc sites was determined in the zincophosphate CoZnPO–CZP, in a five-wavelength study using data from ELETTRA.

Keywords: anomalous scattering; MAD; metal atom occupancy; aluminophosphates; molecular sieves.

1. Introduction

Synchrotron radiation availability in recent years has allowed great advances to be made in structural chemistry. The high intensity, wavelength tunability and exceptional vertical collimation of synchrotron radiation, coupled with advances in detector technology including image plates and, more recently, fast-readout CCD detectors, have led to these advances. High-resolution powder diffraction data allow *ab initio* structure determinations and refinements to be carried out. The high intensity of synchrotron radiation is also used for the data collection from microcrystals, and other weakly diffracting single-crystal samples, for example, at station 9.8 at Daresbury Laboratory, which is dedicated to such experiments. Moreover, the collection of data for deformation density studies, which requires carefully measured data to very high resolution and minimizing systematic errors, can be achieved rapidly by selection of short-wavelength radiation and use of a CCD detector. The Laue method uses white radiation and a stationary crystal, and data can be collected rapidly using relatively few images; small-molecule crystal structures can be solved and refined to give satisfactory results, and the Laue method is particularly applicable to crystals which tend to decay, as well as for time-resolved studies. The wavelength tunability is harnessed for resonant diffraction experiments which are used primarily in valence contrast and selective atom diffraction, including neighbouring-element contrast experiments. It is on this topic which this article concentrates. A general review is given and then two case studies from my own work are described.

2. Resonant diffraction

The distinction between neighbouring atoms in the periodic table by conventional single-wavelength (*e.g.* Mo *Kα* and Cu *Kα*) X-ray diffraction techniques is often not feasible since their X-ray scattering factors are very similar. This problem becomes even more acute when two or more such atoms occupy a single site, each at partial occupancy. In contrast, the scattering power of atoms in the diffraction of neutrons is only weakly dependent on the atomic number of the atoms, but can vary widely between adjacent atoms in the periodic table, and so in favourable cases can enable neighbouring-atom identification to be made, *e.g.* manganese has a negative neutron scattering length whereas that of iron is positive.

With the advent of intense synchrotron X-ray sources for use in X-ray diffraction studies, anomalous dispersion techniques can harness the wavelength tunability of synchrotron radiation to uniquely identify atom sites, for

elements with absorption edges which are accessible to synchrotron radiation. Such experiments are based on the large changes of the X-ray atomic scattering factor, close to the absorption edge, due to the variations in f' and f'' with wavelength,

$$f = f^0 + f' + if'',$$

where f^0 is the scattering factor of the unperturbed atom, and f' and f'' are the real and imaginary parts of the anomalous scattering.

The energy of the absorption edge is quite different for elements close together in the periodic table. Therefore, identification and location of different elements is possible (sometimes at low occupancy), even when such elements occupy the same site. The method involves collection of diffraction data at two or more wavelengths at which there are significant differences in the atomic scattering factor. For example, selective atom diffraction was used to determine the bismuth distribution in the superconductor 2212 Bi–Sr–Ca–Cu–O using two data sets, one of which was collected at a wavelength at the lower part of the bismuth edge and a second at a wavelength well below the edge (Lee et al., 1989). This choice of wavelengths minimized the variation in f'' but induced a change in f' of about 9e and allowed the determination of 5% and 6% of Bi in the Sr and Ca sites, respectively. In a study of $Co_2Fe(PO_4)_2$ (Warner et al., 1991), which has five- and six-coordinate metal atoms sites, the value of f' for Fe at the wavelength chosen for data collection, close to the Fe absorption edge, was determined to be −7.81 (9), using the known structure of $Fe_3(PO_4)_2$ (Fig. 1). This result was then utilized to show that there is a preference for Co to occupy the penta-coordinate site, with refined values for the occupancies of Fe in close agreement with a neutron diffraction study. A similar comparison of neutron and resonant methods was given in the determination of the cation distribution in $NiFe_2(PO_4)_2$ (Warner et al., 1995). Perkins & Attfield (1991) determined the cation distribution in $FeNi_2BO_5$
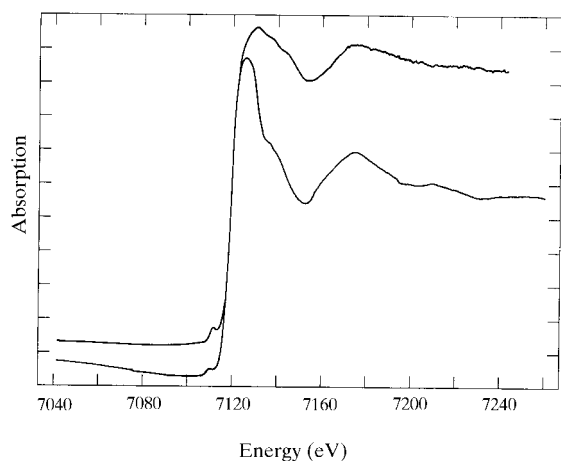
using powder diffraction data measured 16 eV below the Fe K-absorption edge and using α-Fe_2O_3 as a standard to refine the value of f'(Fe). The occupancies of the four metal atom sites were refined independently to give final values quite different to the statistically predicted quantities, but close to those found in $AlNi_2BO_5$, showing that charge, rather than size, directs the cation populations. The distribution of Zn and Na cations over the possible cation sites in Zn/Na zeolite Y was determined using data measured close to the Zn K-edge and at a wavelength remote from the Zn absorption edge at 0.8 Å (Wilkinson et al., 1992). It was found that the possible cation sites were occupied by either Zn or Na, but not both (Fig. 2), and the occupancies obtained were in close agreement with those found by chemical analysis.

Anomalous dispersion experiments can distinguish between valence states of different sites of an element, using the valence contrast method, since the absorption edge of an atom is shifted by a few eV, depending on its valence state (generally there is a 2–6 eV increase in energy for an increase in oxidation number of 1). For instance, Attfield (1990) determined the sites of the two Eu^{3+} and one Eu^{2+} site in Eu_3O_4 using data collected close to the Eu L_{III}-edge. In addition, the cation and valence distribution in $EuSm_2O_4$ was resolved. $GaCl_2$ is a mixed-valence $Ga^IGa^{III}Cl_4$ compound, and by measurement of powder diffraction data at several wavelengths close to the Ga edge position it was shown that there is an oxidation shift of up to 8 eV between the two valence states (Wilkinson et al., 1991). By refining f' at each site for the different data sets it was possible to identify the valence state of each site. This work was extended in a comparison of the spectra of $GaCl_2$, $GaAlCl_4$ and $GaCl_3$, where Ga has valence I in $GaAlCl_4$ and valence III in $GaCl_3$, Fig. 3 (Wilkinson & Cheetham, 1992). Fe^{2+} and Fe^{3+} sites were distinguished in α-Fe_2PO_4 by measuring powder diffraction data at three different wavelengths, two of which were close to the f' minimum for Fe^{2+} and Fe^{3+}, respectively, and the third at a wavelength remote from the edge positions (Warner et al., 1992). Refining f' at each of the two Fe sites allowed the
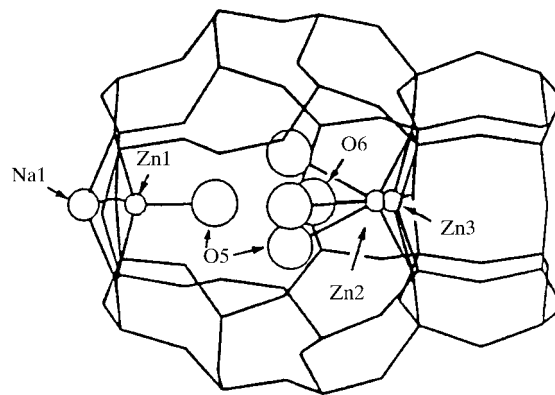

Figure 1
XANES spectra of $Fe_3(PO_4)_2$ (upper) and $Co_2Fe(PO_4)_2$ (lower) (from Warner et al., 1991).

Figure 2
The structural model found for the cation positions in Zn/Na zeolite Y (from Wilkinson et al., 1992).

distinction between valence state at the two sites to be made. In a single-crystal study of (μ-dioxo)Mn(2,2′-bipyr-idyl)$_2$(BF$_4$)$_3$.3H$_2$O, which contains Mn(III) and Mn(IV) cations, f' curves were obtained for each Mn site using 24 reflections measured at eight different energies around the Mn K-edge, whose relative shift was about 4 eV (Gao *et al.*, 1992). In similar experiments conducted on single crystals, an Nb(VI) and two Nb(IV) sites were identified in NbSe$_3$ (Gao *et al.*, 1993), and Fe^{2+} and Fe$^{2.5+}$ sites were assigned in Fe$_3$O$_4$ (Sasaki *et al.*, 1998).

The absorption-edge position is also affected by the coordination of the element in question. An example is shown in a series of anomalous dispersion experiments conducted on the garnet Y$_3$Ga$_3$Ga$_2$O$_{12}$, which contains octahedrally and tetrahedrally coordinated Ga^{3+} ions. These show distinct X-ray scattering behaviour in the near-edge region, and significant differences in f' [see Wilkinson *et al.* (1991), with further details in Cheetham & Wilkinson (1992)]. In some cases there is a dependence of the edge
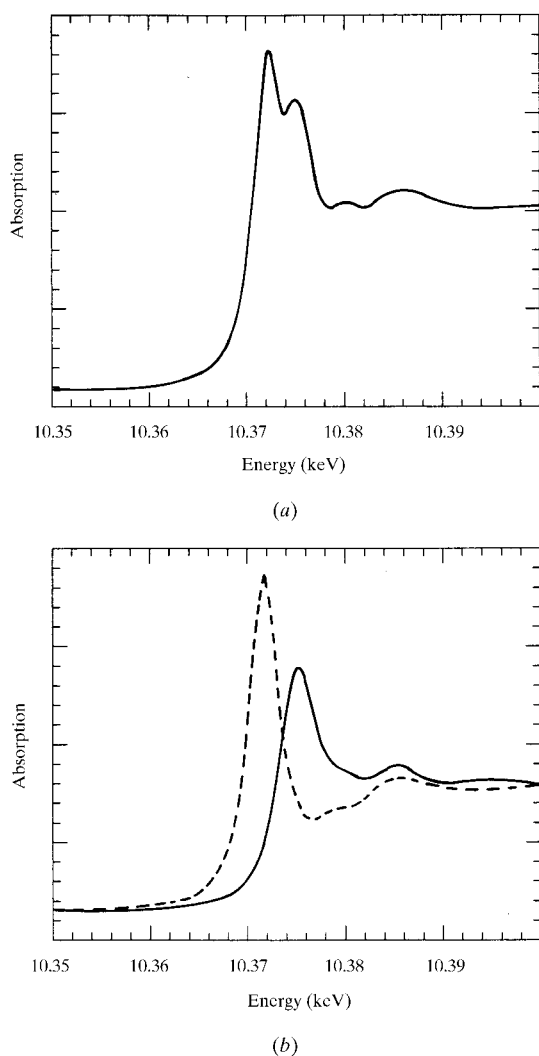
position and XANES effect on the orientation of the crystal, arising from an asymmetric environment about a bound atom. An example of this effect is seen in the square-planar tetrachloroplatinate ion, Fig. 4 (Templeton & Templeton, 1985).

Anomalous scattering has been widely used in protein crystallography. In one of the first examples, Mn^{2+} and Ca^{2+} sites were resolved in pea lectin by data collection close to the Mn K-edge and a data set away from the absorption edge, allowing the calculation of anomalous difference Fourier maps, based on the large relative difference in f'' (Einspahr *et al.*, 1985). The so-called MAD method (Hendrickson, 1991) is used as a new way of solving the protein structure. For the developments of SRS, ESRF, CHESS and ELETTRA for MAD, see Cassetta *et al.* (1999). Such methods have also been demonstrated for the solution of small-molecule crystal structures, although they are generally not required, with the powerful modern programs for structure solution from normal diffraction data (see, for example, Chapuis *et al.*, 1985; Templeton & Templeton, 1987; Fischer & Pilz, 1997). In the latter paper a new method was used to determine the partial structure of each of two anomalous scatterers, Se and Sb, in a centro-symmetric crystal of Cu$_3$SbSe$_3$. The method may find application to the solving of structures which give two or more non-unique solutions by conventional methods, or structures which converge to a false minimum. The possible application to *ab initio* structure determination from powder diffraction data, using the Patterson method, where one particular difficulty is the exact coincidence of Friedel pairs of reflections, and the overlap of other reflections, was suggested by Prandl (1990). For a centrosymmetric case,

(a)

(b)

Figure 3
(a) X-ray absorption spectrum of GaCl$_2$. (b) X-ray absorption spectra of GaAlCl$_4$ (broken line) and GaCl$_3$ (solid line) (from Wilkinson & Cheetham, 1992).
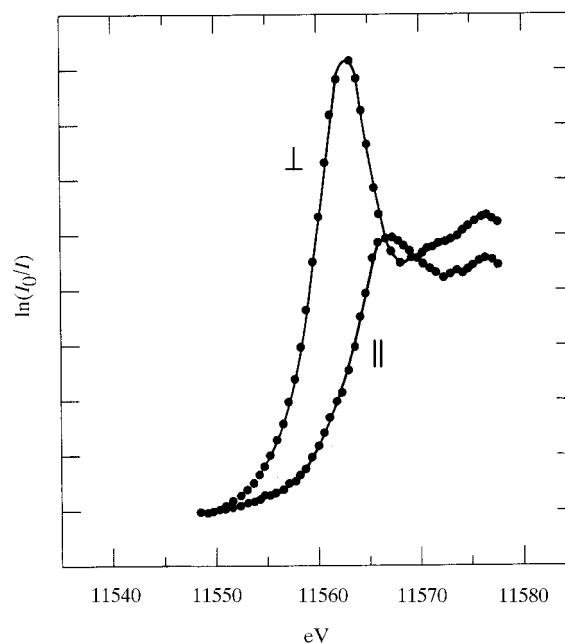

Figure 4
Pt L_3 absorption edge for PtCl$_4^{2-}$, with the electric vector of the polarized X-rays parallel or perpendicular to the fourfold axis of PtCl$_4^{2-}$ (from Templeton & Templeton, 1985).

one anomalous scatterer and powder data measured at two wavelengths, one at the absorption edge, is sufficient. For non-centrosymmetric samples, two types of anomalous scatterer are required, and data measured at three different wavelengths, two of which have contributions from one or other of the anomalous scatterers. The method has recently been demonstrated for the centrosymmetric case using $SrSO_4$ as a test sample (Burger *et al.*, 1998). The Sr atom was found using an f' difference Patterson, and this was used to phase 71 resolved unique reflections by maximum entropy methods to allow the remainder of the structure to be solved (Fig. 5).

3. Determination of metal incorporation in two phosphate-based microporous materials

My interest in resonant diffraction experiments has focused principally on its application to microporous materials, such as aluminophosphates and other phosphate-based molecular sieves, and the work has been carried out in collaboration with V. Kaucic and his group in Ljubljana, Slovenia. These materials are related to zeolites but tend to have significantly different surface selectivities. They have found increasing importance in recent times due to their activity as solid acid catalysts, which tend to be more selective and avoid the environmentally harmful reagents of the older processes. Their activity is a complex function of the framework charge, the shape and size of the pores within the structures, and the nature of metal atoms incorporated into the framework. Aluminophosphates have an uncharged framework, but the substitution of divalent metal atoms into the framework, which tends to take place at the aluminium sites, places a negative charge

on the framework, in turn giving rise to possible catalytic activity. In order to gain insight into the role of the metal atom sites in the physical–chemical properties it is essential to study the nature and position of these sites within the framework. Such an understanding should in turn lead to the possibility of synthesizing materials with desired properties. The determination of such metal atom sites in these materials is a challenging problem, since two or more metal atoms which are close together in atomic number may be incorporated at the same site, and often to an extent of just a few percent. Moreover, the crystals tend to be small and weakly diffracting. In this paper, experiments on two such materials will be described.

4. NiAPO – a test case

NiAPO is an aluminophosphate which was expected to have the APO-21 structure. The crystal structure analysis was determined using data measured using a Cu $K\alpha$ rotating-anode diffractometer, which showed it to have a novel layer structure, Fig. 6 (Helliwell *et al.*, 1993). The Ni atoms fully occupy octahedral sites in the framework, and are bonded to two ethylene diamine molecules, one monodentate and the other bidentate. The remaining coordination is given by two framework O atoms and a water molecule, and the Ni atoms form links between the aluminophosphate layers. A second data set was collected using Mo $K\alpha$ radiation and, since the difference in f' between Mo $K\alpha$ and Cu $K\alpha$ for Ni is 3.3e, it was possible to determine the Ni atom position by calculating an f' difference Fourier map. Clearly the signal could be enhanced by collecting data close to the K-absorption edge for nickel, using synchrotron radiation, in order to optimize
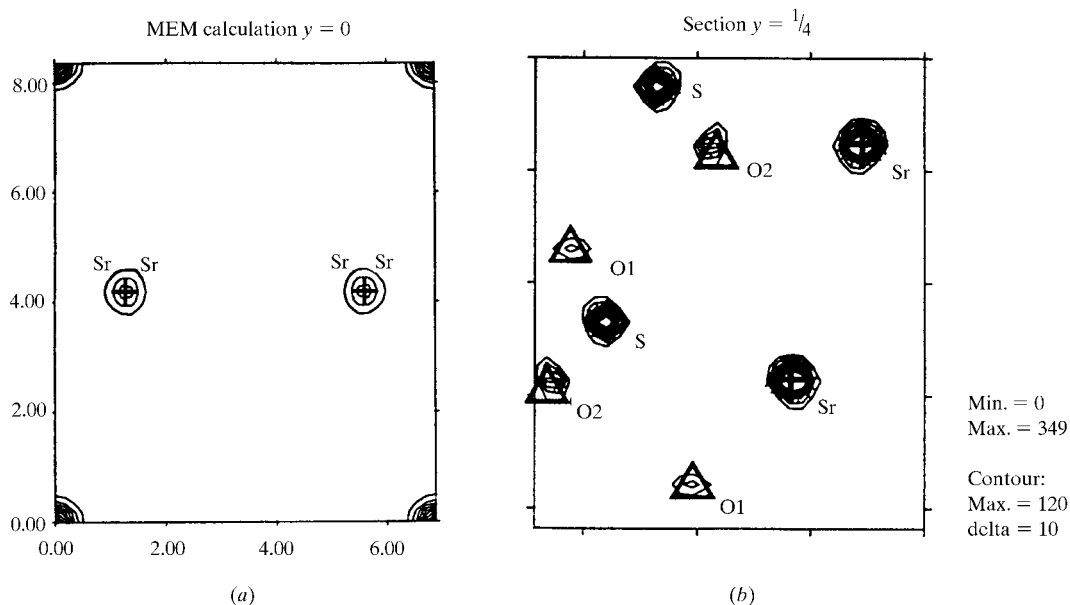

Figure 5
(*a*) Partial Patterson density of Sr atoms in $SrSO_4$, from two near-edge measurements. (*b*) Electron density distribution of $SrSO_4$, found using maximum entropy methods (from Burger *et al.*, 1998).

the difference in f' for Ni. Therefore, data were subsequently collected at the NSLS (National Synchrotron Light Source), at a wavelength close to the f' dip, which was determined by means of a transmission spectrum from a powder sample (Fig. 7). Helliwell *et al.* (1996) reports these experiments. The wavelength selected for data collection was 0.0007 Å (3.9 eV) removed from the f' dip on the low-energy side (to avoid high absorption by nickel and complications with XANES or EXAFS variation on f'),
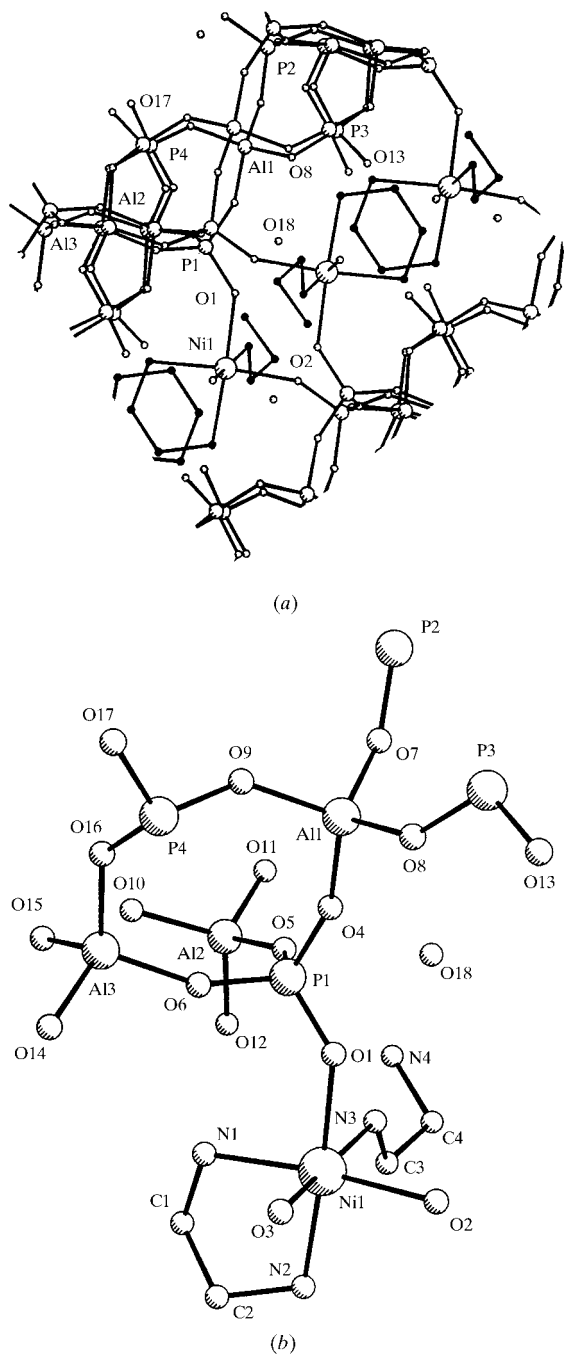
giving an expected value for f' of $-7.6e$ (Sasaki, 1989). Table 1 summarizes some key facts for the three data sets.

In order to calculate the f' difference Fourier maps it was then necessary to scale the data sets. Data scaling on F in orthogonal directions of reciprocal space (*i.e.* anisotropic scaling) was achieved using the program *SCALEIT*, which is part of the CCP4 program suite (Collaborative Computational Project, Number 4, 1994). The results are shown in Table 2. Final ratios of the mean value of $F_{\lambda 1}{}^2$ to $F_{\lambda 2}{}^2$ were close to unity, and the R and wR values for the Cu $K\alpha$ to Mo $K\alpha$ data were reasonable, with the lower wR value reflecting that it is only the weak data which gives ratios which are not close to unity. The R and wR values for the scaling of the synchrotron radiation data to either of the rotating-anode data sets were high, reflecting in part the larger difference in f' between data sets, but also arising from some partial decay to the crystal which took place during and after the synchrotron radiation data collection.

(a)

(b)

Figure 6
(*a*) A section of the crystal structure of NiAPO, showing the layer structure. (*b*) The asymmetric unit of NiAPO (from Helliwell *et al.*, 1993).
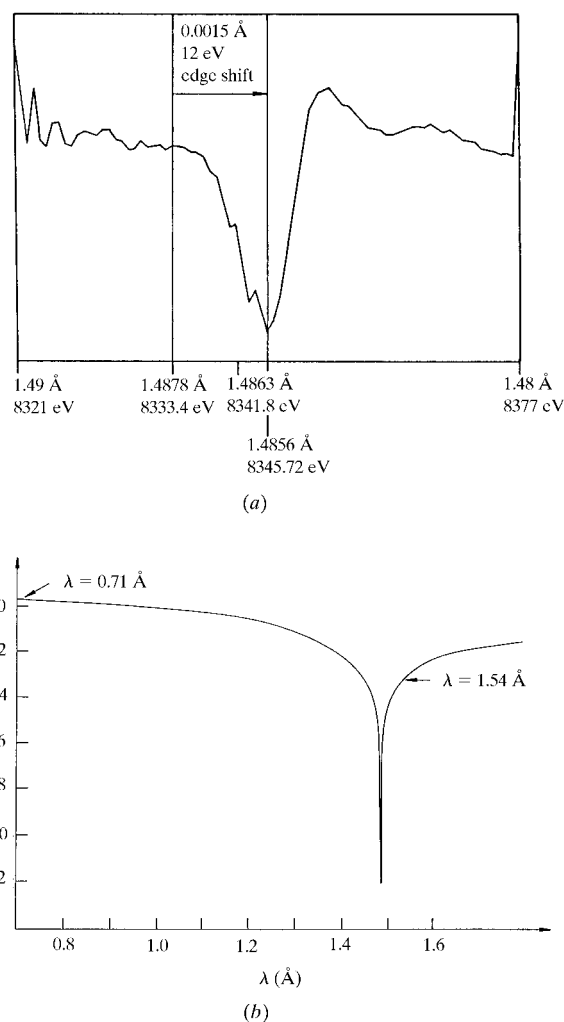

(a)

(b)

Figure 7
(*a*) Absorption edge dip (1.4856 Å) for NiAPO measured at NSLS, with the wavelength for the data collection (1.4863 Å) indicated. (*b*) Theoretical values for the free atom (Sasaki, 1989) (from Helliwell *et al.*, 1996).

Table 1
Crystal data for NiAPO (from Helliwell *et al.*, 1996).

		Cu $K\alpha$ rotating anode,	Mo $K\alpha$ rotating anode,
Formula		$NiAl_3P_4O_{18}C_4H_{21}N_4$	
Space group		$P2_1/n$	
Crystal size (mm)		$0.25 \times 0.05 \times 0.02$	
Radiation, wavelength (Å)	Synchrotron, 1.4863	1.54178	0.71069
No. of reflections:			
Independent	1596	4601	4745
Observed	1452	3497	2681
D_{min} (Å)	1.1	0.78	0.78
R	0.152	0.057	0.067
No. of parameters	138	309	308

In order to calculate the f' difference Fourier maps it was necessary to obtain a suitable phase set, and this was achieved using the Cu $K\alpha$ data set, and either carrying out refinement with the Ni atom excluded or with Al substituted at the Ni atom site. It was found that the latter phase set produced optimum results, without introducing bias, and so these results will be described and are summarized in Table 3. f' difference Fourier maps were computed using *FFT* (Collaborative Computational Project, Number 4, 1994), which were placed on an absolute scale by using the scale factors obtained in the *SHELXL93* (Sheldrick, 1992) refinements. In each case a peak was obtained which was close to the refined Ni atom site and whose peak height and position reflected the value of $\Delta f'$ between the two wavelengths, *i.e.* $|F_{Mo\,K\alpha} - F_{SR}| > |F_{Cu\,K\alpha} - F_{SR}| > |F_{Mo\,K\alpha} - F_{Cu\,K\alpha}|$ (SR = synchrotron radiation). The $|F_{Mo\,K\alpha} - F_{SR}|$ map gave the optimum coordinate accuracy, as one would expect for the larger signal.

The $\Delta f'$ values estimated from the peak heights, using the known $\Delta f'$ value of 3.3e from the $|F_{Mo\,K\alpha} - F_{Cu\,K\alpha}|$ peak as a reference, were systematically higher than expected for the Cu $K\alpha$ or Mo $K\alpha$ minus the synchrotron radiation data. It was thought that this was because some decay had occurred to the crystal during the lengthy four-circle diffractometer synchrotron radiation data collection (approximately one week). This caused an apparent reduction of occupancy of the Ni atom due to the lowering of its order, therefore leading to an enhancement of the $\Delta f'$ values. The decay was evidenced by a significant change in the unit-cell dimensions, seen during the course of the synchrotron radiation data collection, and also in a subsequent additional collection of Cu $K\alpha$ data using the rotating-anode diffractometer. For the latter data set the number of observed reflections was approximately halved, compared with the Cu $K\alpha$ data collected prior to the synchrotron radiation run. Moreover, refinement of the structure using either the synchrotron radiation or the second Cu $K\alpha$ data set showed that there was a marked decrease in the order of the structure, and a reduction of the apparent occupancy of the Ni atom to between 0.6 and

Table 2
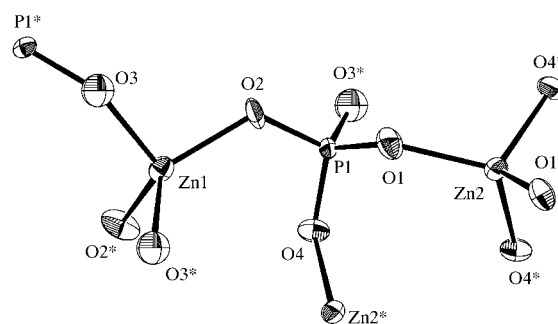Data scaling for one data set to another for NiAPO (from Helliwell *et al.*, 1996).

SR = synchrotron radiation.

Data sets	Final scale (mean $F_{\lambda 1})^2$/(mean $F_{\lambda 2})^2$	R-factor	Weighted R-factor
SR to Mo $K\alpha$	1.003	0.367	0.199
SR to Cu $K\alpha$	1.004	0.319	0.363
Cu $K\alpha$ to Mo $K\alpha$	0.986	0.164	0.111

0.7. In order to avoid such problems, data collection using an image plate or CCD is indicated, so that data collection times can be greatly reduced, and two or more wavelengths can be obtained much more rapidly and using the same apparatus. In this way, problems with sample decay, as well as beam or wavelength instabilities, should be minimized. Snell *et al.* (1995) had previously demonstrated the use of an image plate with a small crystal of NiAPO. Such an experiment is described in the following section.

5. CoZnPO–CZP

CoZnPO–CZP is a small-pore molecular sieve, whose composition is $Na_6[Co_{0.2}Zn_{0.8}PO_4]_6(H_2O)_6$. Its structure was determined using Mo $K\alpha$ radiation, in 1995 by Zabukovec Logar *et al.* (1995), which showed that it had a novel chiral topology and therefore could have applications in enantiomeric separations, reactivity or catalytic activity. A new refinement was carried out using data collected in Manchester using Cu $K\alpha$ radiation, which allowed the absolute configuration to be determined, and some key parameters from this structure determination are shown in Table 4 (Helliwell *et al.*, 1999). The framework contains two crystallographically different metal atom sites (Fig. 8), and replacement of approximately 20% of the Zn atom content by cobalt was known to have taken place from the chemical analysis (and also indicated by the bright blue colour of the crystals). However, owing to the lack of scattering contrast between cobalt and zinc at Mo $K\alpha$ or Cu $K\alpha$ wavelengths, the refinement in either case gave little indication of the

Figure 8
An *ORTEP* (Johnson, 1965) plot of a portion of CoZnPO–CZP, omitting the non-framework atoms for clarity (from Helliwell *et al.*, 1999).

Table 3
Results of f' difference Fourier calculations for NiAPO (from Helliwell *et al.*, 1996).

SR = synchrotron radiation.

Data	Peak	r.m.s	Relative peak height	Estimate of $\Delta f'$†	Expected $\Delta f'$‡	Distance from refined Ni atom position (Å)
Mo $K\alpha$ − SR	18.0	0.7	2.6	8.6	7.8	0.025
Cu $K\alpha$ − SR	13.8	0.6	2.0	6.6	4.5	0.057
Mo $K\alpha$ − Cu $K\alpha$	6.9	0.3	1	–	3.3	0.189

† This is derived from the relative peak height values, and assuming Mo $K\alpha$ − Cu $K\alpha$ is 3.3e.   ‡ From Sasaki (1989).

Table 4
Crystal data for CoZnPO–CZP (from Helliwell *et al.*, 1999).

Formula	$Na_6[Co_{0.2}Zn_{0.8}PO_4]_6(H_2O)_6$
Space group	$P6_522$
Radiation, wavelength (Å)	Cu $K\alpha$ rotating anode, 1.54178
Crystal description	Blue prismatic
Crystal size (mm)	$0.05 \times 0.02 \times 0.02$
No. of reflections:	
Independent	713
Observed	637
D_{min} (Å)	0.89
$R, wR[F^2]$	0.0513, 0.1252
No. of parameters	72

Table 5
Summary of the five data sets collected at ELETTRA from a crystal of CoZnPO–CZP (from Helliwell *et al.*, 1999).

Data set	Zn f'	Zn f''	1.45 Å	Co f'	Co f''
Wavelength (Å)	1.2846	1.2840	1.4500	1.6083	1.6073
Resolution limit (Å)	1.44	1.44	1.62	1.80	1.80
Measured reflections	2008	2014	1347	970	957
Unique reflections (Bijvoets separate)	170	175	119	84	85
R_{merge} (F)	0.082	0.159	0.065	0.062	0.079

distribution of substituted Co over the two sites. For example, for the Cu $K\alpha$ data, refinement of the occupancies of Co set to x and y at the Zn1 and Zn2 sites, respectively, was attempted, with populations of Zn constrained to $1 - x$ and $1 - y$ at these two sites. This resulted in occupancies for Co of 19 (3)% at Zn1 and 13 (3)% at Zn2, indicating that there may be more cobalt at the Zn1 position. Since the difference is not significant, however, full occupancies by zinc were assumed for the final rounds of refinement. Clearly, the only way to resolve this problem was to pinpoint the site(s) of incorporation using anomalous dispersion techniques to target the zinc and cobalt contents specifically, using synchrotron radiation data measured at their respective K-absorption edges.
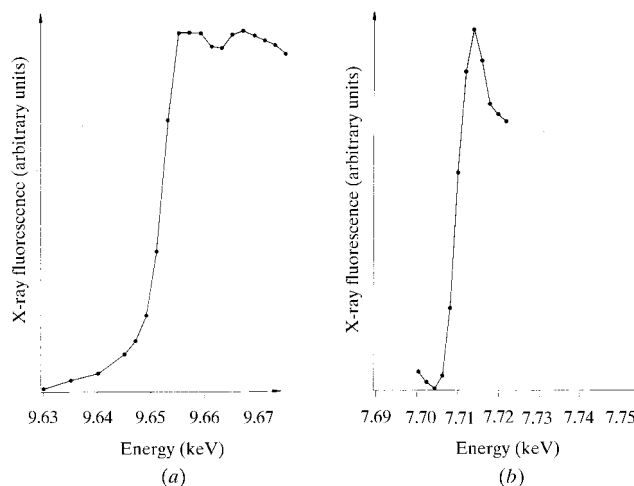
The synchrotron radiation experiments were carried out at ELETTRA. Fluorescence scans were measured directly from the crystal (which was subsequently used for all the data collection), to determine the positions of the K-edges of both Zn and Co. These are shown in Fig. 9. For zinc the position of the f' dip, half way up the absorption edge, was found to be at a wavelength of 1.2846 Å, while the position of the f'' maximum, at the top of the white line, was found to be at 1.2840 Å. For Co, the f' dip was at 1.6083 Å and the f'' maximum was at 1.6073 Å. About 180° sample rotation for the diffraction data were then collected at each of these four wavelengths, using a MAR image plate of diameter 180 mm. A fifth data set was collected at a wavelength of 1.45 Å, *i.e.* at a wavelength remote from each of the K-absorption edges. The detector was placed as close as possible to the crystal, but the small aperture of the MAR placed a limit on the recordable resolution, owing to the

long wavelengths used. The resolution limits were 1.44 Å for data measured at the Zn absorption edge, 1.62 Å for data measured at 1.45 Å and only 1.8 Å for data measured at the Co K-edge. Thus the final processed sets of unique data (with Bijvoets separate and overloads removed) consisted of somewhat limited numbers of reflections (Table 5).
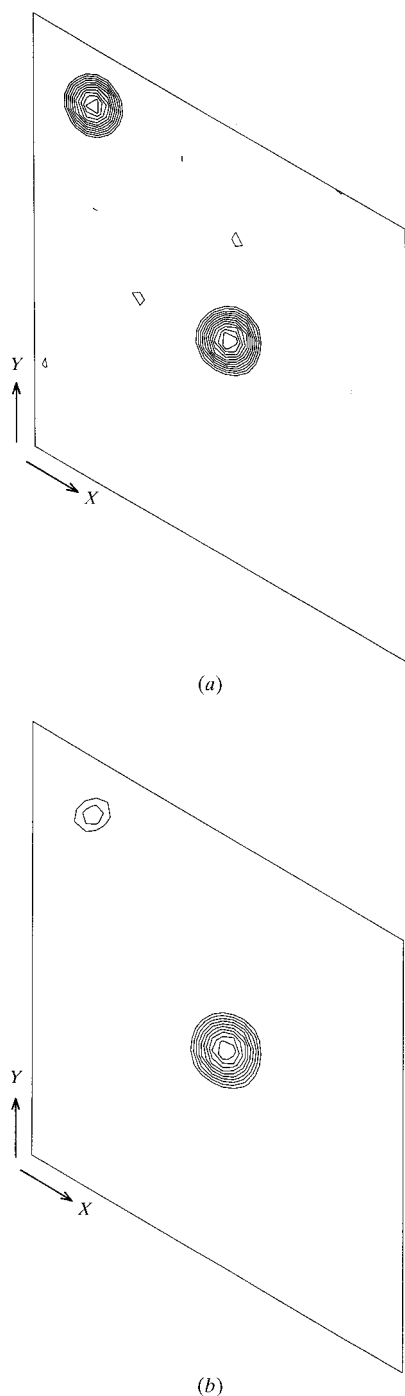
Data scaling was carried out using *SCALEIT*. After a number of computational trials it was found that optimal scaling could be achieved using a small subset of reflections which were essentially wavelength independent. Suitable reflections were located using *SFALL* (Collaborative

Figure 9
Edge scans measured from the crystal of CoZnPO–CZP at ELETTRA (from Helliwell *et al.*, 1999) (*a*) at the Zn K-edge, (*b*) at the Co K-edge.

Table 6
Results from FFT for CoZnPO–CZP (from Helliwell *et al.*, 1999).

Data	Peak height/ r.m.s. at M1 site	Peak height/ r.m.s. at M2 site	Distance from refined Zn1 site (Å)	Distance from refined Zn1 site (Å)
1.45 Å Zn f'	7.89	7.20	0.107	0.084
1.45 Å Co f	6.88	2.75	0.100	0.104

(*a*)

(*b*)

Figure 10
Dispersive difference Fourier maps (from Helliwell *et al.*, 1999) (*a*) using the coefficients $|F_{1.45\,Å} - F_{Zn f'}|$, (*b*) using the coefficients $|F_{1.45\,Å} - F_{Co f'}|$.

Computational Project, Number 4, 1994) by generating three sets of calculated structure factors, based on Zn1, Zn2 and Zn1 plus Zn2 as the models. A subset of six reflections with significant intensities in the measured data sets, but which had F_{Zn} values close to zero in all three calculated sets, was selected since these had essentially no contribution from the metal and were therefore wavelength independent. These reflections were then used to determine an overall scale factor for the scaling of the f' data for Zn and Co to the data measured at 1.45 Å. The use of wavelength-independent reflections was particularly important for the scaling of the Zn f' data, since the r.m.s isomorphous difference (calculated in *SCALEIT*) was 22.15, whereas it was only 2.67 for the scaling of the Co f' data to the 1.45 Å data.

Suitable phase sets were generated using the model from the Cu $K\alpha$ refinement, firstly assuming 100% Zn at the two metal atom sites and secondly with phosphorus replacing the metal atoms. Results using either phase set were similar, so those using the former phase set will be described and are summarized in Table 6. The f' difference Fourier maps were calculated using *FFT* (Fig. 10). Two significant peaks were obtained in the map using the coefficients $|F_{1.45\,Å} - F_{Zn f'}|$, which were close to the two metal atom sites. The one at the M1 site was a little higher than that at the M2 site. The map calculated using the coefficients $|F_{1.45\,Å} - F_{Co f'}|$ gave only one significant peak, close to the M1 site. There is a small feature at the M2 position, which was the fifth highest peak on the map, but this is less than three times the r.m.s. value, and therefore is not significant.

Thus, from the $|F_{1.45\,Å} - F_{Co f'}|$ map, the site of incorporation has indeed been determined as M1, as previously indicated in the laboratory-based refinements. However, the Zn peak at this site is higher than that at M2 in the $|F_{1.45\,Å} - F_{Zn f'}|$ map. This result was inconsistent with the Co $\Delta f'$ map. In order to resolve this ambiguity, refinement of the occupancy for zinc at the two sites was carried out using the program *MLPHARE* (Collaborative Computational Project, Number 4, 1994). The 'native' data set was defined as the Zn f' dip data, with the other four data sets used as 'derivatives', so that refinement was carried out against $|F_{derivative} - F_{Zn f'}|$. In each case the peak at the M2 site refined to a higher content than that at the M1 site, with the value approximately reflecting the difference in f' between the particular wavelength pair (Table 7). These refined occupancies indicate that the Co content at the M1 site is between 24 and 30%, whilst that at the M2 site is between 10 and 16%. The fact that the peak height order

Table 7
Refinement of zinc occupancies for CoZnPO–CZP using *MLPHARE* (from Helliwell *et al.*, 1999).

'Derivative'†	$\Delta f'$ (e)‡	Refined Zn occupancy at M1 site	Refined Zn occupancy at M2 site	Ratio of Zn1/Zn2 occupancies
Zn f'	3.8	0.067	0.078	0.86
1.45 Å	9.6	0.164	0.181	0.91
Co f'	10.2	0.138	0.154	0.9
Co f'	10.2	0.130	0.169	0.77

† The native data set was that measured at the Zn f' dip.   ‡ $\Delta f'$ is the theoretical $[f'_{derivative} - f'_{native}]$ (Sasaki, 1989) and refinement of the occupancy was against $|F_{derivative} - F_{Zn\,f'}|$.

was wrong in the Zn f' difference map must have arisen from the limited resolution of the data sets, owing to the small aperture of the MAR image plate. In order to avoid this problem, a cylindrical image plate or a CCD mounted on a 2θ goniostat arm would be better.

6. Final comments

These experiments demonstrate that it is indeed possible to identify and determine the occupancies of one or more metal atom types, which are close together in atomic number and present at the same sites using multiple-wavelength anomalous dispersion techniques. In the NiAPO paper (Helliwell *et al.*, 1996) it was deduced that an occupancy of 10% nickel should give a significant signal, assuming a $\Delta f'$ of 7.8e for the fully occupied Ni atom site in NiAPO. Thus the method should be sensitive to a resonant signal difference down to about one electron when the data quality and resolution limits are good. Optimization of the instrumentation involving the area-detector provision is therefore desirable, especially when absorption edges of interest are at long wavelengths, and the diffraction pattern expands to higher Bragg angle, and where at least 1 Å resolution would be advantageous. In a new study of MnAPO-50, which contains two metal sites, each partially occupied by Al and Mn, a Cu $K\alpha$ refinement gives an indication of the proportion of Mn at each site. Clearly, however, data collection close to the Mn K-edge (at a wavelength of approximately 1.89 Å) would be needed for obtaining a more precise value for the Mn occupancies, if a suitable detector arrangement was available.

References

Attfield, J. P. (1990). *Nature (London)*, **343**, 46–49.
Burger, K., Cox, D., Papoular, R. & Prandl, W. (1998). *J. Appl. Cryst.* **31**, 789–797.
Cassetta, A., Deacon, A. M., Ealick, S. E., Helliwell, J. R. & Thompson, A. W. (1999). *J. Synchrotron Rad.* **6**, 822–833.
Chapuis, G., Templeton, D. H. & Templeton, L. K. (1985). *Acta Cryst.* A**41**, 274–278.
Cheetham, A. K. & Wilkinson, A. P. (1992). *Angew. Chem. Int. Ed. Engl.* **31**, 1557–1570.
Collaborative Computational Project, Number 4 (1994). *Acta Cryst.* D**50**, 760–763.
Einspahr, H., Sugana, K., Suddath, F. L., Ellis, G., Helliwell, J. R. & Papiz, M. Z. (1985). *Acta Cryst.* B**41**, 336–341.
Fischer, K. F. & Pilz, K. (1997). *Acta Cryst.* A**53**, 475–483.
Gao, Y., Frost-Jensen, A., Pressprich, M. R. & Coppens, P. (1992). *J. Am. Chem. Soc.* **114**, 9214–9215.
Gao, Y., Pressprich, M. R. & Coppens, P. (1993). *Acta Cryst.* A**49**, 216–219.
Helliwell, M., Gallois, B., Kariuki, B. M., Kaucic, V. & Helliwell, J. R. (1993). *Acta Cryst.* B**49**, 420–428.
Helliwell, M., Helliwell, J. R., Cassetta, A., Hanson, J. C., Kvick, A., Kaucic, V. & Frampton, C. (1996). *Acta Cryst.* B**52**, 479–486.
Helliwell, M., Helliwell, J. R., Kaucic, V., Zabukovec Logar, N., Barba, L., Busetto, E. & Lausi, A. (1999). *Acta Cryst.* B**55**, 327–332.
Hendrickson, W. A. (1991). *Science*, **254**, 51–58.
Johnson, C. K. (1965). *ORTEP*. Report ORNL-3794. Oak Ridge National Laboratory, Tennessee, USA.
Lee, P., Gao, Y., Sheu, H. S., Petricek, V., Restori, R., Coppens, P., Darovskikh, A., Phillips, J. C., Sleight, A. W. & Subramanian, M. A. (1989). *Science*, **244**, 62–63.
Perkins, D. A. & Attfield, J. P. (1991). *J. Chem. Soc. Chem Commun.* pp. 229–231.
Prandl, W. (1990). *Acta Cryst.* A**46**, 988–992.
Sasaki, S. (1989). KEK Report 88–14. National Laboratory for High Energy Physics, Tsukuba, Japan.
Sasaki, S., Toyoda, T., Yamawaki, K. & Ohukubo, K. (1998). *J. Synchrotron Rad.* **5**, 920–922.
Sheldrick, G. M. (1992). *SHELXL93. Program for Crystal Structure Refinement.* University of Gottingen, Germany.
Snell, E., Habash, J., Helliwell, M., Helliwell, J. R., Raftery, J., Kaucic, V. & Campbell, J. W. (1995). *J. Synchrotron Rad.* **2**, 22–26.
Templeton, D. H. & Templeton, L. T. (1985). *Acta Cryst.* A**41**, 365–371.
Templeton, D. H. & Templeton, L. T. (1987). *Acta Cryst.* A**43**, 573–574.
Warner, J. K., Cheetham, A. K. & Cox, D. E. (1995). *J. Appl. Cryst.* **28**, 494–502.
Warner, J. K., Cheetham, A. K., Cox, D. E. & Von Dreele, R. B. (1992). *J. Am. Chem. Soc.* **114**, 6074–6080.
Warner, J. K., Wilkinson, A. P., Cheetham, A. K. & Cox, D. E. (1991). *J. Phys. Chem. Solids*, **52**, 1251–1256.
Wilkinson, A. P. & Cheetham, A. K. (1992). *J. Appl. Cryst.* **25**, 654–657.
Wilkinson, A. P., Cheetham, A. K. & Cox, D. E. (1991). *Acta Cryst.* B**47**, 155–161.
Wilkinson, A. P., Cheetham, A. K., Tang, S. C. & Reppart, W. J. (1992). *J. Chem. Soc. Chem Commun.* pp. 1485–1487.
Wilkinson, A. P., Cox, D. E. & Cheetham, A. K. (1991). *J. Phys. Chem. Solids*, **52**, 1257–1266.
Zabukovec Logar, N., Rajic, N., Kaucic, V. & Golic, L. (1995). *J. Chem. Soc. Chem Commun.* pp. 1681–1682.